Cite this: DOI: 10.1039/xxxxxxxxxx

Director configuration in the twist-bend nematic phase of CB11CB

Isabella Miglioli,[a] Corrado Bacchiocchi,[*b] Alberto Arcioni,[a] Alexandra Kohlmeier,[c] Georg H. Mehl,[c] and Claudio Zannoni[a]

Received Date
Accepted Date

DOI: 10.1039/xxxxxxxxxx

www.rsc.org/journalname

The director distribution in the nematic phases exhibited by the 1″,11″-bis(4-cyanobiphenyl-4′-yl)undecane (CB11CB) liquid crystal has been studied in the bulk with the EPR spin probe technique. EPR spectra confirmed the presence of an higher temperature uniaxial nematic phase and of a lower temperature nematic phase in which the director distribution is not uniform. Spectra recorded in the lower temperature nematic phase were not fully compatible with theoretical EPR spectra calculated according to the recently proposed model for the twist-bend phase in which the local domain director twists around an axis with a fixed tilt angle, θ_0, but were well described by a "distributed-tilt" model in which the director has a relatively narrow distribution, centred at θ_0.

1 Introduction

The presence of a second, lower temperature nematic phase in banana-shaped liquid crystals (LCs) made by two cyanobiphenyl mesogenic units linked by an odd-membered alkyl chain (odd symmetric LC dimers) was first observed by Panov et al.[1]. The basic structural features of this phase for the odd symmetric LC dimer homologue 1″,7″-bis(4-cyanobiphenyl-4′-yl)heptane (CB7CB) were then proposed by Cestari et al.[2] who suggested the phase to be the twist-bend nematic (N_{tb}) phase originally proposed by Meyer[3] and theoretically predicted by Dozov for banana-shaped mesogens[4]. In particular, Cestari et al.[2] described the phase as macroscopically uniaxial with a local nematic director that makes a constant tilt angle θ_0 with the macroscopic axis and twists around it in an helical fashion. Equal regions of opposite twist are expected to be present making the whole system achiral.

In the following years a number of studies on odd symmetric LC dimers, in particular CB7CB, have supported the twist-bend model for the lower temperature nematic phase. These works include, in particular, a detailed 2D NMR study[5]; a comparison of a molecular field model of the phase to NMR quadrupolar splittings[6]; electro-optic measurements[7,8]; DSC and optical polarization microscopy[9]; freeze-fracture TEM[8,10,11] and hi-res cryo-TEM[11]; synchrotron X-ray diffraction[10] and birefringence measurements[12]. A recent work by Tamba et al.[13] combined optical polarization microscopy, small-angle X-ray scattering and electron microscopy to study the nanostructure and the filament formation properties of a LC phase of a symmetric difluoroterphenyl dimer below the N_{tb} phase.

As the twist-bend model for the lower temperature nematic phase gained general consensus, studies emerged trying to elucidate the main features responsible for the onset of the phase and even if the main mechanism responsible for the N_{tb} phase is still an open question, some agreement on empirical observations is emerging. In a recent two-part review on the relationship between molecular structure and the formation of the N_{tb} phase, Mandle et al.[14,15] concluded that the overall bent shape of the molecule is more important than electrostatic interactions that nonetheless play a role and must be in a "Goldilocks" range. Similar conclusions have been reached in previous theoretical[16] and experimental[17–19] works.

Despite the general agreement, the local director configuration of the N_{tb} phase is still debated[20,21] and a more direct evidence that the director distribution in these materials is exactly of the type indicated by several authors as the heliconical twist-bend is still missing and worth investigating[9,22,23].

The EPR spin probe technique[24–26] seems to be well suited to test the proposed structure of the N_{tb} phase and, in principle, would be an independent approach to estimate the constant tilt angle θ_0. In fact, the analysis of the spectra of a suitable stable nitroxide free radical dissolved in the LC host can provide molecular-level information about the ordering, the reorientational dynamics and the local nematic director configuration sensed by the probe in the N_{tb} phase.

[a] *Dipartimento di Chimica Industriale "Toso Montanari", Università, Viale Risorgimento 4, I-40136 Bologna, Italy*
[*b] *School of Science and Technology, Chemistry Division, University of Camerino, Via S. Agostino 1, I-62032 Camerino (MC), Italy, Fax: +39 0737 637 345; Tel: +39 0737 40 2260; E-mail: corrado.bacchiocchi@unicam.it*
[c] *Department of Chemistry, University of Hull, Hull HU6 7RX, UK*

Until now the only EPR measurements on this type of dimers we are aware of have been done by Cestari et al. in their seminal article[2] on the homologue CB7CB. In a qualitative assessment of the EPR spectra the Authors pointed out that in the N phase the spectra are consistent with a nematic monodomain whose director is parallel to the magnetic field whereas in the N_{tb} phase the spectra change significantly indicating a nonuniform alignment of the director. A detailed analysis of the EPR spectra was however not presented at the time.

Given the proposed structure of the N_{tb} phase, this spectral change is not the expected one since, on cooling from a nematic monodomain, it appears reasonable that the axis of the N_{tb} phase, around which the director twists with the constant tilt angle θ_0, would be parallel to the magnetic field of the EPR spectrometer, as it has been determined in NMR measurements on CB7CB[27]. The expected spectrum in the N_{tb} phase should therefore correspond still to a monodomain whose director is tilted at an angle θ_0 with respect to the magnetic field.

To check if this spectral change is common to other odd symmetric LC dimer homologues, this article presents a detailed investigation of 1″,11″-bis(4-cyanobiphenyl-4′-yl)undecane (CB11CB) in the bulk and provides evidence from the analysis of EPR spectra that seems to be at variance with the proposed description of the N_{tb} phase[2,5–8,10–12,27].

The structure of the article is as follows. In the next section experimental details are provided. The Theory section describes the models used to analyse the EPR spectra. Information recovered from the analyses are then presented in the Results and Discussion section and a summary of the main findings is reported in the Conclusions section.

2 Experimental

The LC dimer CB11CB is formed by two cyanobiphenyl groups linked by an alkyl chain of eleven carbon atoms. It was synthesized in the Department of Chemistry at the University of Hull (UK) and was used without further purification. Its molecular structure is shown in Figure 1.

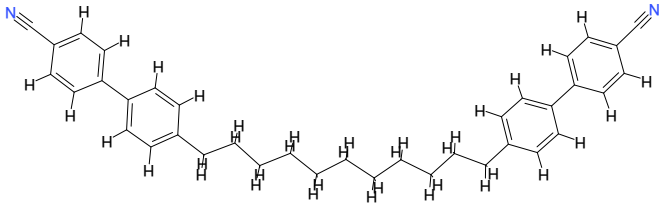

Fig. 1 Molecular structure of CB11CB.

This material, upon cooling from the isotropic (I) phase, exhibits a transition to the ordinary, uniaxial nematic phase (N_u) and, on further cooling, to a second nematic phase, described as a N_{tb} phase. Phase sequence reported by various authors varies slightly[1,9,28–30].

The phase sequence of the CB11CB LC used in this work, determined on heating by DSC at 10 K/min, was: Crystal – 377.2 K – N_{tb} – 381.9 K – N_u – 398.5 K – I.

The nitroxide spin probe, used for doping the CB11CB LC, was the 3β-doxyl-5α-cholestane free radical (Aldrich, hereafter referred to as CSL). This was employed in a number of previous studies[25,31–33] where it proved to be a reliable probe to monitor the order and the dynamics of the LC system, due to its size, morphology and rigidity, which results in a strong orientation by the LC host. The CSL structure is shown in Figure 2 together with the chosen ordering (x,y,z, solid line) and magnetic (x',y',z', dashed line) molecular frames and the indication of its two main reorientational motions, tumbling and spinning, with the corresponding components of the rotational diffusion tensor: $D_\perp$ (reorientation of the molecular long axis) and $D_\parallel$ (rotation around the long axis), respectively.

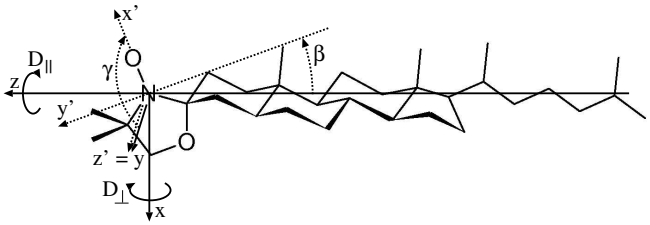

Fig. 2 Molecular structure of the CSL spin probe together with the chosen ordering (x,y,z, solid line) and magnetic (x',y',z', dashed line) molecular frames, the Euler angles, β and γ, between the molecular frames and the principal components, $D_\perp$ (reorientation of the molecular long axis) and $D_\parallel$ (rotation around the molecular long axis), of the rotational diffusion tensor.

CSL was added to CB11CB in the I phase at a typical concentration of about 1×10^{-4} g_{CSL}/g_{CB11CB}, which is below the limiting concentration typically suggested[24] to avoid Heisenberg spin exchange distortion effects.

Samples of CSL-doped CB11CB were inserted into glass capillaries of 1.8 mm internal diameter for the EPR measurements. EPR spectra were acquired with a Bruker EMX spectrometer equipped with an ER 041XG microwave X-band (9.5 GHz) Gunn Diode bridge and a rectangular ER 4102ST cavity. The samples were thermostated with a nitrogen flux through a variable temperature unit Bruker B-VT 2000. The temperature was monitored with a calibrated type T thermocouple (Comark Ltd.) kept in close proximity with the sample and showed a stability better than ±0.05 K.

The molecular magnetic frame (x',y',z') was chosen according to the standard system of coordinates for the N–O paramagnetic moiety with the x' axis along the N–O bond[31,34] and the z' axis perpendicular to the five-membered ring, i.e. parallel to the p_z orbital containing the unpaired electron. According to a standard approach, the z axis of the molecular ordering frame is considered parallel to the principal axis of inertia of the probe (its "long axis") and, to simplify the rotation which takes the ordering into the magnetic frame[31,34], the y axis is considered parallel to the z' axis. To reduce the correlation among variable parameters, the Euler angles, β and γ, between the molecular frames, were fixed in the fittings to 15° and 90°, respectively, in agreement with previous results obtained in related systems[25,31–34].

The EPR spectra simulation program employed was based on a set of Fortran routines implementing the slow tumbling the-

ory for a spin probe reorienting in a LC, developed by Freed and collaborators[24,35,36], combined with a software package[37] that optimizes the fit parameters using the Gauss-Newton-Marquardt non-linear least squares method[38].

On cooling from the I to the N_u phase, from 393.2 K, down to 379.2 K, spectra were very well fitted by a simple monodomain aligned along the magnetic field, indicating that the spectrometer field is able to produce an essentially ($\approx$ 95%) uniform sample (see the Results and Discussion section for details). In the presence of the magnetic field, this uniformity is expected to be maintained upon the further cooling into the N_{tb} phase.

3 Theory

The nitroxide spin probe is assumed to reorient in a locally uniaxial nematic domain whose director, $\boldsymbol{n}$, can be oriented, in general, at an angle β_d with respect to the spectrometer uniform magnetic field. The corresponding unsaturated, high-field EPR spectrum, $I_N(\omega-\omega_0,\beta_d)$, at frequency ω, is calculated using the classic Stochastic Liouville Equation approach of Freed and collaborators[24,35,36] which predicts that:

$$I_N(\omega-\omega_0,\beta_d)=\frac{1}{\pi}\langle\langle v|\left[(\hat{\mathbf{\Gamma}}-i\mathscr{L})+i(\omega-\omega_0)\boldsymbol{I}\right]^{-1}|v\rangle\rangle\,, \qquad (1)$$

where the central frequency, ω_0, at the spectrometer field, B_0 (0.339 T), is obtained from the g factor, g_0, and the Bohr magneton, β_e: $\omega_0=g_0\beta_e B_0/\hbar$. $\mathscr{L}$ is the Liouville superoperator obtained from the orientation dependent spin Hamiltonian, $\hat{\mathbf{\Gamma}}$ is the diffusion superoperator describing the reorientational motion of the probe, $|v\rangle$ is a vector containing spin transition moments averaged over the equilibrium ensemble and $\boldsymbol{I}$ is the identity. A brief account of the general approach of Freed and collaborators[24,35,36] has been presented in a previous work[25]. To reduce the total number of model parameters, the reorientational motion of the probe is assumed to take place in a uniaxial, mean field ordering potential

$$U(\beta)=-kT\left[\lambda_{20}P_2(\cos\beta)\right]\,, \qquad (2)$$

where λ_{20} is the strength of the potential, k the Boltzmann constant, T the temperature in Kelvin and $P_2(\cos\beta)$ is a second rank Legendre polynomial. The local order is described by the orientational order parameter, $\langle P_2\rangle$, defined as

$$\langle P_2\rangle=\frac{\int P_2(\beta)\exp[-U(\beta)/kT]\sin\beta\,\mathrm{d}\beta}{\int\exp[-U(\beta)/kT]\sin\beta\,\mathrm{d}\beta}\,, \qquad (3)$$

where β is the probe orientation with respect to the local domain director.

The EPR spectrum of a spin probe in a LC phase, that can be modelled as a distribution of uniaxial nematic domains, is given by the superposition of the monodomain spectra, $I_N(\omega-\omega_0,\beta_d)$

$$I_T(\omega-\omega_0)=\int_{\beta_d} I_N(\omega-\omega_0,\beta_d)P(\beta_d)_T\,\mathrm{d}\beta_d\,, \qquad (4)$$

where $I_T(\omega-\omega_0)$ is the theoretical EPR spectrum, $P(\beta_d)_T$ is the distribution of the local nematic director and the integral extends over the entire variation of β_d.

In the N_{tb} phase the local nematic domain director is supposed to precess uniformly about an axis, making a fixed angle, θ_0, with it[6,8,10,12,27,39]. A "fixed-tilt" (FT) model can be defined accordingly, indeed, when the axis is oriented along the magnetic field, the local director is uniformly oriented at a fixed angle θ_0 and the director distribution is simply a tilted delta function, $P(\beta_d)_{FT}=\delta(\beta_d-\theta_0)$.

When the axis is perpendicular to the magnetic field, as indicated in Figure 3, the local director, $\boldsymbol{n}$, is uniformly distributed on the surface of a cone of aperture $2\theta_0$ whose axis is perpendicular to the laboratory z axis, taken as the direction of the magnetic field. In this case, $P(\beta_d)_{FT}$ can be obtained as follows.

A is the projection of P onto the xz plane and B is the projection of P onto the z axis. Assuming $\overline{OP}$ unitary, we have: $\overline{OA}=\sin\theta_0$ and $\overline{OB}=\cos\phi\sin\theta_0$. Since we have also $\overline{OB}=\cos\beta_d$, β_d and ϕ can be related as $\cos\beta_d=\cos\phi\sin\theta_0$.

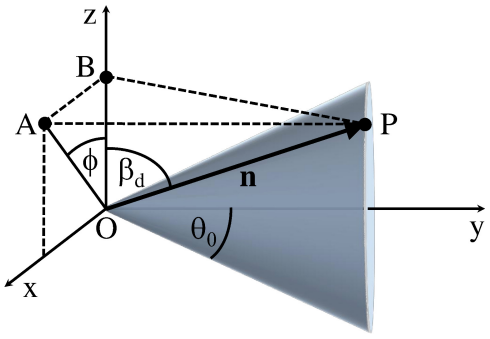

Fig. 3 Schematic of the conical distribution of the local director in the twist-bend model when the cone axis is perpendicular to the z axis, taken as the direction of the magnetic field.

The conical distribution must obey the relation

$$P(\beta_d)_{FT}\,\mathrm{d}\beta_d=P(\phi)\,\mathrm{d}\phi, \qquad (5)$$

therefore

$$P(\beta_d)_{FT}=P(\phi)\frac{\mathrm{d}\phi}{\mathrm{d}\beta_d}=\frac{1}{2\pi}\frac{\mathrm{d}\phi}{\mathrm{d}\beta_d}, \qquad (6)$$

since the distribution of the angle ϕ is uniform. To calculate $\frac{\mathrm{d}\phi}{\mathrm{d}\beta_d}$ we obtain ϕ from the previous relation

$$\phi=\arccos\frac{\cos\beta_d}{\sin\theta_0}. \qquad (7)$$

Finally we obtain

$$\frac{\mathrm{d}\phi}{\mathrm{d}\beta_d}=\frac{\csc\theta_0\sin\beta_d}{\sqrt{1-\cos\beta_d^2\csc\theta_0^2}}. \qquad (8)$$

$P(\beta_d)_{FT}$ is real for $\frac{\pi}{2}-\theta_0<\beta_d<\frac{\pi}{2}+\theta_0$. A second rank order parameter, $\langle P_2\rangle_d$, corresponding to this director distribution can be introduced as

$$\langle P_2\rangle_d=\frac{\int_{\frac{\pi}{2}-\theta_0}^{\frac{\pi}{2}+\theta_0}\left[\frac{3}{2}\cos^2(\beta_d)-\frac{1}{2}\right]P(\beta_d)_{FT}\,\mathrm{d}\beta_d}{\int_{\frac{\pi}{2}-\theta_0}^{\frac{\pi}{2}+\theta_0}P(\beta_d)_{FT}\,\mathrm{d}\beta_d}=\frac{1}{8}[-1-3\cos(2\theta_0)]. \qquad (9)$$

The dependence of the $\langle P_2\rangle_d$ of the distribution upon the angle θ_0 shows the expected behaviour. In particular, when $\theta_0\to 0$ the

distribution reduces to a monodomain perpendicular to the magnetic field and the $\langle P_2\rangle_d$ assumes the limiting value $-1/2$; when $\theta_0 \to \pi/2$ the distribution becomes uniform on the xz plane and the limiting value of $\langle P_2\rangle_d$ is $1/4$.

As presented in the Results and Discussion section, the analyses of the EPR spectra done with the FT model failed to provide a consistent temperature behaviour of the parameters recovered from the fits. The main problem with the FT model seemed to be the following. When the axis of the N_{tb} phase is parallel to the magnetic field, the EPR spectrum should be just a tilted monodomain, since the local domain director twists around the axis with a constant tilt angle θ_0. Instead, the experimental spectra in the N_{tb} phase were clearly of the polydomain type.

A conceivable model that maintains the basic structure of the twist-bend phase and is also compatible with polydomain EPR spectra is one in which the local domain director is not fixed at θ_0 with respect to the magnetic field but is described by a relatively narrow distribution, centred at θ_0. The relevant angular distribution for this "distributed-tilt" (DT) model has been obtained as follows.

The uniform magnetic field is oriented along the z axis of the lab reference frame x,y,z (Figure 4). The uniform tilt direction of the twist-bend phase is defined by the z' axis of a second reference frame, x',y',z', rotated with respect to x,y,z by the Euler angles $0,\theta_0,0$. The local domain director, $\boldsymbol{n}$, is taken as a unitary vector having, in the x',y',z' frame, coordinates $\sin\phi\cos\alpha, \sin\phi\sin\alpha, \cos\phi$. The angle between the director, $\boldsymbol{n}$, and the magnetic field is β_d.

The unknown probability density distribution of the director, $\boldsymbol{n}$, in the x',y',z' frame, is assumed to be uniaxial, centred on the z' axis, with a uniform distribution of α, $P(\alpha) = 1/2\pi$, whereas the distribution of the polar angle ϕ is modelled, as it is usually done (e.g. in the EPRLL "family" of EPR spectra simulation programs[40]) by a P_2-type distribution, $P(\phi) \propto \exp[\lambda_d P_2(\cos\phi)]$, where P_2 is a second rank Legendre polynomial and λ_d is a positive constant.

The order of the domain director with respect to z' is described by the orientational order parameter, $\langle P_2\rangle_d$, defined as

$$\langle P_2\rangle_d = \frac{\int P_2(\cos\phi)\,\exp[\lambda_d P_2(\cos\phi)]\,\sin\phi\,d\phi}{\int \exp[\lambda_d P_2(\cos\phi)]\,\sin\phi\,d\phi}. \qquad (10)$$

A value of $\langle P_2\rangle_d = 0$ represents the limiting case of an isotropic distribution of the domain directors, corresponding to $P(\beta_d)_{DT} = 1/\pi$, whereas in the other limit of $\langle P_2\rangle_d = 1$, the local director is uniformly oriented at a fixed angle θ_0 and the director distribution becomes identical to the previous model, $P(\beta_d)_{DT} = P(\beta_d)_{FT} = \delta(\beta_d - \theta_0)$.

An explicit equation for the probability density distribution of the angle β_d can be obtained by expressing ϕ in terms of β_d by noticing that $\cos\beta_d$ and $\cos\phi$ are the z and z'coordinates of $\boldsymbol{n}$, respectively (see Figure 4), related by

$$\cos\beta_d = \sin\theta_0\sin\phi\cos\alpha + \cos\theta_0\cos\phi. \qquad (11)$$

The expression of ϕ in terms of β_d is obtained, after some algebra, as

$$\cos^2\phi = f(\alpha,\beta_d) = \frac{\sec^2\theta_0\left(\cos\beta_d - \cos\alpha\tan\theta_0\sqrt{\cos^2\alpha\sin^2\theta_0 - \cos^2\beta_d + \cos^2\theta_0}\right)^2}{\left(1+\cos^2\alpha\tan^2\theta_0\right)^2}. \qquad (12)$$

The probability density distribution of the angle β_d is therefore

$$P(\alpha,\beta_d)_{DT} = \exp\left[\lambda_d\left(\frac{3}{2}f(\alpha,\beta_d) - \frac{1}{2}\right)\right]. \qquad (13)$$

The integration of this expression along both α and β_d is carried out numerically using the adaptive multidimensional integration Fortran routine DCUHRE[41].

It is worth pointing out that such a distribution of tilt angles with respect to the magnetic field is not necessarily the only one that could fit the spectra. The reason is that a magnetic resonance experiment like our one is only sensitive to the angle between a molecular magnetic tensor axis and the spectrometer magnetic field direction. It is conceivable that another distribution could, for example, describe a situation in which the helical axis, although parallel on average to the magnetic field, is undulating while the tilt angle is fixed with respect to the helix axis[42]. However, yet another possibility is that of a more inhomogeneous distribution of fluctuations of the helix axis as well as of tilt angles. Any model of this type would, however, require additional fitting parameters and, we believe, its introduction would not be justified by our current observable results. We thus stick, following Occam's razor principle, to the minimal deviation from the standard heliconical model that fits our spectra.

4 Results and Discussion

The ability of the CSL spin probe to report correctly the local nematic order of the CB11CB LC can be assessed by noticing that CSL was able to consistently report the local order and the director organization of the 5CB LC in previous studies[43,44]. It has also been shown by Oganesyan et al., using molecular dynamics simulations of the CSL probe in 5CB[45], that the order parameter of the probe and of the mesogen are in good agreement. If the local environment in which the CSL spin probe is located is similar in these two different but related LCs, it is reasonable to expect that CSL will report correctly the local nematic order also of the CB11CB LC.

In Figure 5 a typical rigid-limit spectrum of CB11CB, recorded in the bulk, is compared with typical rigid-limit bulk spectra of 1″,9″-bis(4-cyanobiphenyl-4′-yl)nonane (CB9CB) and of 5CB. For every LC the spectrum was recorded at a temperature well be-

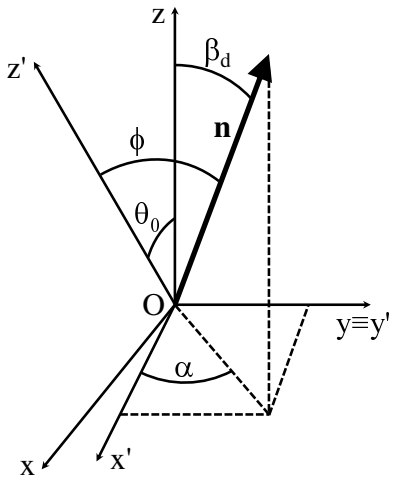

Fig. 4 Schematic of the geometrical relation between $\cos(\beta_d)$ and $\cos(\phi)$ as the z and z' coordinates of the local domain director $\boldsymbol{n}$ (see text for details).

low the relative melting temperature, T_m, and in the rigid-limit regime. The resulting reduced temperatures, $T^* \equiv T/T_m$, were thus 0.733 for CB11CB, 0.616 for CB9CB and 0.586 for 5CB. Melting temperatures, observed on heating, were 377.2 K for CB11CB, 362.15 K for CB9CB and 295.7 K for 5CB. Apart from a small difference in the linewidths, the position of the peaks, which is determined solely by the hyperfine tensor which, in turn, is dependent on the polarity of the environment, is the same in the three LCs indicating that (i) the rigid-limit spectrum of CB11CB is typical of these kind of dimeric LCs and that (ii) the local environment in which the CSL spin probe is located should be fairly similar in 5CB and in CB11CB.

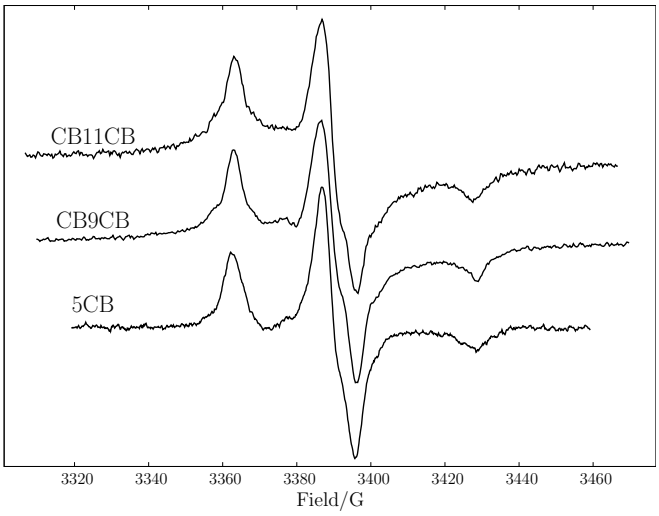

Fig. 5 Typical rigid-limit spectrum of CB11CB, recorded in the bulk at the reduced temperature, $T^* \equiv T/T_m$, of 0.733, compared with a typical rigid-limit bulk spectrum of CB9CB at $T^* = 0.616$ and with a typical rigid-limit bulk spectrum of 5CB at $T^* = 0.586$. T_m is the melting temperature observed on heating which is 377.2 K for CB11CB, 362.15 K for CB9CB and 295.7 K for 5CB.

Final EPR spectra were recorded, on cooling, in the temperature interval 403.2–368.2 K to study the isotropic and the nematic phases (see below) exhibited by the CB11CB LC. EPR spectra recorded between 403.2 and 395.2 K had three well-resolved hyperfine lines typical of a relatively fast motional isotropic regime, without other contributions, clearly indicating that the CB11CB was in the I phase. These spectra were consistently fitted to the isotropic model. Two spectra typical of the I phase at 403.2 and 395.2 K are shown in Figure 6 (top spectra, black line) together with the corresponding fits (red line).

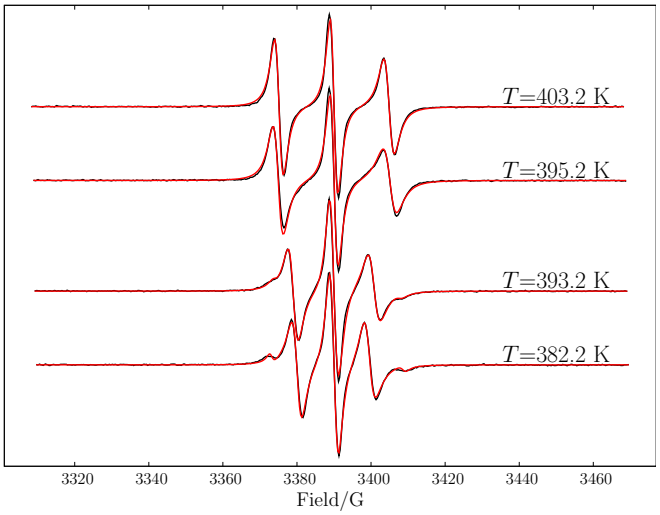

Fig. 6 Typical EPR spectra (black line) in the I phase (top two spectra) and in the N_u phase (bottom two spectra). Top spectra are fitted (red line) to an isotropic model; bottom spectra are fitted to a nematic monodomain model with a small contribution (about 5 %) of an isotropic distribution of domains (see text for details).

By lowering the temperature at 393.2 K, the position of the outermost peaks, previously constant, suddenly changed, indicating that a phase transition had occurred. The approximate temperature of this transition was 394.2 K, about 4 K below the T_{NI} of CB11CB not doped with CSL, measured via DSC on heating. A downshift of the transition temperature of a few K has been observed in previous works on the related LC CB7CB[5,46] in presence of a small amount of a dopant. The observed spectral lineshapes were typical of a N_u phase, as expected, with the director uniformly aligned along the magnetic field. Two spectra typical of the N_u phase at 393.2 and 382.2 K are shown in Figure 6 (bottom spectra, black line). A very small contribution, determined in the analysis to be about 5 %, can be seen as shoulders or peaks at the extremes of the main spectrum. In the temperature interval 393.2–379.2 K, the main spectrum was modelled as a uniaxial nematic monodomain obtaining a consistent temperature dependence of the best-fit parameters. The small outer peaks were not compatible with the isotropic model and were approximately reproduced with the DT model, with parameters $\langle P_2 \rangle_d = 0$ and tilt angle $\theta_0 = 0°$, which corresponds to an isotropic distribution of domains. The nature of this contribution, being quite small, could not be determined more accurately. Fits of the spectra at 393.2 and 382.2 K are also shown in Figure 6 (bottom spectra, red line).

In a series of preliminary analyses, spectra in the range 378.2–376.7 K showed a progressively lower uniaxial nematic spectral contribution and a new, increasing, contribution. This behaviour

suggested the presence in our CSL-doped CB11CB LC of a biphasic region in which the N_u and the N_{tb} phases coexist over a temperature interval of a few K. A coexistence region, induced by a small amount of a dopant, was indeed observed in previous works on the related LC CB7CB[5,46]. This coexistence is consistent with the first order nature of the N_{tb}–N_u transition in these materials, as reported by Tripathi et el.[47] for the dimer homologue CB9CB. Below 376.7 K the uniaxial nematic spectral contribution was no longer present, suggesting that the system was fully in the lower temperature N_{tb} phase. In this phase, spectra showed additional hyperfine contributions at low and high field, indicating a nonuniform alignment of the director with respect to the magnetic field. A similar behaviour has been found by Cestari et al.[2] who recorded a series of EPR spectra across the N_u and N_{tb} phases of CB7CB.

Before any attempt to analyse the spectra in the coexistence region could be made, it was necessary to model the spectra in the lower temperature N_{tb} phase.

Spectra recorded between 375.7 and 372.2 K were quite similar, thus confirming that the system was not experiencing further phase changes. The spectrum recorded at 372.7 K was therefore considered as representative of the N_{tb} phase to be compared against the FT model. The theoretical spectrum was calculated by fixing the FT model parameters at the following values: the local order parameter has been shown[2,5,27] to increase slightly upon entering the N_{tb} phase, accordingly, $\langle P_2 \rangle$ was set at 0.50 which is slightly larger than the value of 0.49 found at the lower end of the N_u phase at 379.2 K; the N_{tb} phase of CB11CB was found to be more viscous than the N_u phase[28], accordingly, to explore a wider dynamical range, the perpendicular component of the rotational diffusion tensor, $D_\perp$, was set at a series of different values between 0.01 ns^{-1} and 0.002 ns^{-1}, which were either half or one tenth of the value of 0.02 ns^{-1} observed at the lower end of the N_u phase, respectively. An estimate of the conical angle, θ_0, for CB11CB has not been reported. The closest available estimate is the conical angle for CB7CB that has been recently determined from the mean value of the ^{2}H NMR quadrupole splittings of CB7CB-d_4 and 8CB-d_2 dissolved in CB7CB[27], from optical birefringence measurements[12] and using transmission electron microscopy[8]. In a range of a few K below the N_{tb}–N_u transition all these studies determined θ_0 to be about 20°. A different estimate of the conical angle for CB7CB, also from optical birefringence measurements[42], determined θ_0 to be about 10°. Following these arguments and to explore a wider range of values, θ_0 was set either at 10° or at 30°.

In Figure 7, top, the EPR spectrum (black line) at 372.7 K in the N_{tb} phase is compared with spectra calculated according to the FT model, with $\langle P_2 \rangle = 0.50$, $D_\perp = 0.01$ ns^{-1} (lower values did not improve the model) and $\theta_0 = 10°$ (red line) or $\theta_0 = 30°$ (green line). The comparison clearly shows that the lineshapes obtained with the FT model are quite different from the experimental spectrum.

To better understand the nature of the director distribution in the N_{tb} phase, spectra at selected temperatures were recorded immediately after "field cooling" (FC) which was done by heating the sample above its T_{NI} then slowly cooling it to the requested temperature at approximately 1 K/min, with the applied magnetic field set at 0.63 T, the highest available on the EPR spectrometer. This procedure should maximise the alignment of the local nematic directors along the magnetic field. A second spectrum was then recorded immediately after a rotation of the sample by 90° around an axis perpendicular to the magnetic field.

In Figure 7, middle and bottom, the EPR spectra (black line) recorded at 370.2 K in the supercooled N_{tb} phase after FC ($\parallel$) and after a 90° rotation of the sample ($\perp$) are presented. At this temperature spectra before and after the rotation were, as expected, clearly different, since the phase is anisotropic and, due to the increased viscosity, the relatively low magnetic field used in the measurements (centred at 0.339 T) was not able to realign the sample. In fact, spectra recorded immediately after the rotation and several hours later were identical (not shown). Since the N_{tb} phase of CB11CB in a standard LC cell was not switched by an electric field lower than 20 V/μm,[9] it seems unlikely that the director distribution will be perturbed by the relatively weak magnetic field of the EPR spectrometer.

These spectra were then compared against the FT model. The theoretical spectra were calculated by fixing the model parameters at the following values: since it has been shown[2,5,27] that, once in the N_{tb} phase, the order parameter $\langle P_2 \rangle$ remains almost constant, it was set at the same previous value of 0.50; since the temperature was only 2.5 K lower than the previous one, the rotational diffusion tensor, $D_\perp$, was also set at the same value of 0.01 ns^{-1}; the conical angle, θ_0, was set, as before, either at 10° or at 30°. This interval should still be appropriate to model the tilt angle that has been reported to maintain a value within 30° in a range of temperatures not too far from the N_{tb}–N_u transition[8,12,27].

In Figure 7, middle and bottom, the EPR spectra (black line) at 370.2 K in the supercooled N_{tb} phase are compared to spectra calculated according to the FT model, with parameter values described above and $\theta_0 = 10°$ (red line) or $\theta_0 = 30°$ (green line). We see that the FT model is able to qualitatively reproduce the spectrum recorded after the rotation ($\perp$), but not the spectrum recorded before the rotation ($\parallel$).

Despite the lack of agreement of spectra calculated according to the FT model with experimental EPR spectra at selected temperatures, an attempt was done to analyse spectra with the FT model, by optimizing fit parameters, from the onset of the biphasic region, at $T = 378.2$ K, to $T = 368.2$ K, in the supercooled N_{tb} phase. To reduce the number of model parameters, different globalization schemes were adopted where the tilt angle, θ_0, was kept variable but was a common parameter to model a group of spectra. In all cases, parameters recovered from the fits failed to show a consistent and meaningful behaviour with temperature, indicating, as expected, that the FT model was not appropriate to correctly reproduce the experimental spectra.

The DT model, presented in the Theory section, was therefore tested against the experimental EPR spectra recorded at 372.7 K in the N_{tb} phase and at 370.2 K in the supercooled N_{tb} phase. In Figure 8, top, the EPR spectrum (black line) at 372.7 K in the N_{tb} phase is compared with spectra calculated according to the DT model, with $\langle P_2 \rangle = 0.50$, $\langle P_2 \rangle_d = 0.44$, $D_\perp = 0.01$ ns^{-1} and $\theta_0 = 10°$ (red line) or $\theta_0 = 30°$ (green line). In the same Figure, middle and

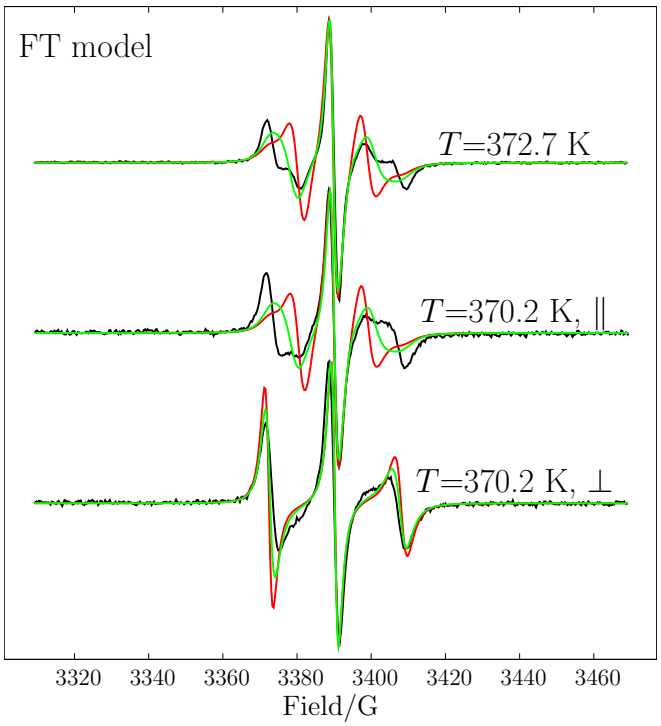

Fig. 7 EPR spectra (black line) at 372.7 K in the N_{tb} phase, top, or at 370.2 K in the supercooled N_{tb} phase, middle and bottom, after FC (||) and after a 90° rotation of the sample around an axis perpendicular to the magnetic field (⊥), compared to spectra calculated according to the FT model with tilt angle $\theta_0 = 10°$ (red line) or $\theta_0 = 30°$ (green line, see text for details).

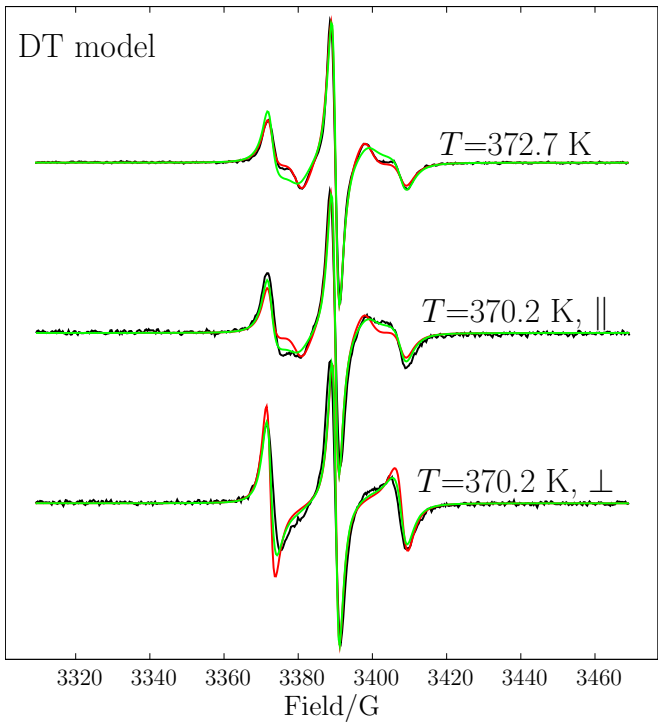

Fig. 8 EPR spectra (black line) at 372.7 K in the N_{tb} phase, top, or at 370.2 K in the supercooled N_{tb} phase, middle and bottom, after FC (||) and after a 90° rotation of the sample around an axis perpendicular to the magnetic field (⊥), compared to spectra calculated according to the distributed-tilt (DT) model with tilt angle $\theta_0 = 10°$ (red line) or $\theta_0 = 30°$ (green line, see text for details).

bottom, the EPR spectra (black line) at 370.2 K in the supercooled N_{tb} phase are compared to spectra calculated according to the DT model, with $\langle P_2 \rangle = 0.50$, $\langle P_2 \rangle_d = 0.40$, $D_\perp = 0.01$ ns^{-1} and $\theta_0 = 10°$ (red line) or $\theta_0 = 30°$ (green line). It is apparent that the lineshapes of the spectra calculated with the DT model resemble more closely those of the experimental spectra compared to the lineshapes of the spectra calculated with the FT model shown in Figure 7.

Experimental spectra recorded in the temperature interval from the onset of the biphasic region, at $T = 378.2$ K, to $T = 368.2$ K, in the supercooled N_{tb} phase, were analysed with the DT model. To reduce the correlation among the fit parameters, separate global analyses were performed for the spectra recorded in the biphasic region, those in the N_{tb} phase and those in the supercooled N_{tb} phase. In each global analysis, the tilt angle, θ_0, and the order parameter of the domain directors, $\langle P_2 \rangle_d$, were global parameters.

With this approach, parameters recovered from the fits appeared to have a variation that was consistent across the biphasic region, the N_{tb} and the supercooled N_{tb} phases and was also consistent with the parameters previously recovered from the I and the N_u phases. The temperature dependence of the local orientational order parameter, $\langle P_2 \rangle$, and of the rotational diffusion tensor, $D_\perp$, across the whole temperature interval studied is shown in Figures 9 and 10, respectively. Recovered global parameters were as follows, biphasic region: $\theta_0 = 16°$, $\langle P_2 \rangle_d = 0.60$; N_{tb} phase: $\theta_0 = 11°$, $\langle P_2 \rangle_d = 0.47$; supercooled N_{tb} phase: $\theta_0 = 20°$, $\langle P_2 \rangle_d = 0.57$.

At the N_{tb}–N_u phase transition, the $\langle P_2 \rangle$ values in the coexistence region (two values on one side of the transition and two on the other) show a very small discontinuity which is within the experimental error, therefore the variation of the $\langle P_2 \rangle$ with the temperature is essentially continuous. This behaviour appears to be in agreement with the theoretical approach of Dozov[4] and the molecular theory proposed by Greco et al.[16].

The observed $\langle P_2 \rangle$ values are also in good agreement with those recently obtained by Zhang et al. from polarized Raman spectroscopy in CB11CB[48] across the N_u phase and immediately below the N_{tb}–N_u phase transition. In particular, Zhang et al. observed, as in our study, that the local $\langle P_2 \rangle$ appears to be continuous across the N_{tb}–N_u phase transition and then remains essentially constant in the N_{tb} phase.

In the supercooled N_{tb} phase, $\langle P_2 \rangle$ values appeared to decrease (see Figure 9, open squares). This was not observed in previous studies on the related dimers CB7CB[27] and CB9CB[20]. A similar behaviour has been observed by Emsley et al. in a recent study on the symmetric difluoroterphenyl dimer DTC5C9[49]. The behaviour of the $\langle P_2 \rangle$ in our study bears another similarity with that observed by Emsley et al. in that it reaches a maximum value in the N_u phase, before the transition to the N_{tb} phase. The decrease of $\langle P_2 \rangle$ values in the N_{tb} phase observed by Emsley et al. was explained as an effect of the simultaneous increase of the tilt angle, θ_0.

Indeed, in our fits, a certain degree of correlation was present between the local $\langle P_2 \rangle$ parameter and the tilt angle, θ_0 and to study this effect, we repeated the spectral fits by assuming that the $\langle P_2 \rangle$ in the supercooled N_{tb} phase had an empirical Haller-type[50] temperature dependence described as

$$\langle P_2 \rangle(T) = \langle P_2 \rangle_0 (1 - T/T_{NI})^{\beta}, \tag{14}$$

where T_{NI} was fixed at 394.2 K, the temperature of the observed N_u–I transition, whereas $\langle P_2 \rangle_0$ and the exponent, β, were obtained by fitting the Haller equation 14 to the $\langle P_2 \rangle$ values in the N_u phase in the range from T_{NI} up to the observed maximum around 383 K (first 7 values, see Figure 9). Best-fit parameters were $\langle P_2 \rangle_0 = 0.70$ and $\beta = 0.09$. The corresponding Haller function is shown as a dashed line in Figure 9.

Best-fit values of the tilt angle, θ_0, recovered from the analysis of the EPR spectra in which the local $\langle P_2 \rangle$ was fixed at the Haller values are shown in the inset of Figure 9 (solid circles). These values of the tilt angle are clearly larger than the value of 20° recovered from previous fits, where θ_0 was treated as a global parameter (see above). The quality of these new fits appears to be slightly lower with respect to the previous ones. As an example, the fit of the spectrum at $T = 371.7$ K, in the supercooled N_{tb} phase, is shown in Figure 11. We notice, however, that a similar increase of the tilt angle upon lowering the temperature in the N_{tb} was also reported for CB7CB from birefringence measurements[51].

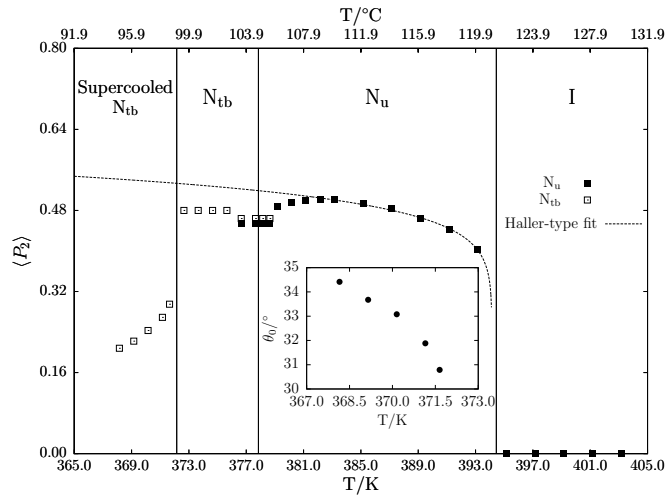

Fig. 9 Temperature dependence of the local orientational order parameter, $\langle P_2 \rangle$, in the I and N_u phase (solid squares) and in the N_{tb} and supercooled N_{tb} phase (open squares), compared with values calculated with the Haller function of eqn. 14 (dashed line, see text for details). The inset shows the temperature dependence of the tilt angle, θ_0 (solid circles), in the supercooled N_{tb} phase recovered from the EPR fits, having fixed the $\langle P_2 \rangle$ at the Haller values. Vertical lines indicate the approximate transition temperatures observed, that are about 4 K below the transitions of CB11CB not doped with CSL, measured via DSC on heating. Four temperature values are in the biphasic region: two on one side of the N_{tb}–N_u phase transition and two on the other.

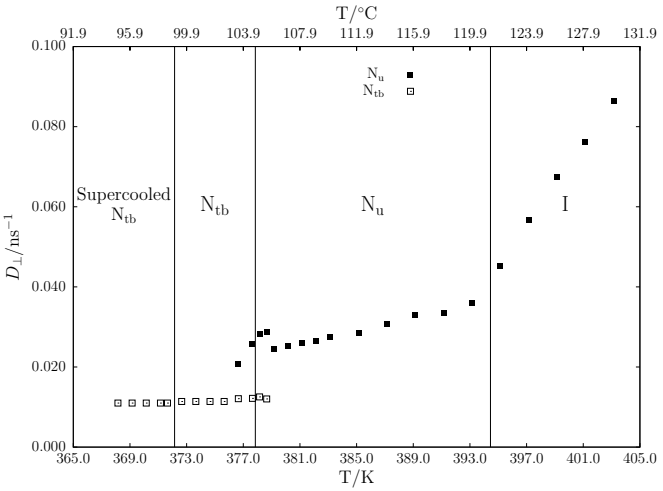

Fig. 10 Temperature dependence of the rotational diffusion tensor, $D_\perp$, in the I and N_u phase (solid squares) and in the N_{tb} and supercooled N_{tb} phase (open squares). Vertical lines indicate the approximate transition temperatures observed, that are about 4 K below the transitions of CB11CB not doped with CSL, measured via DSC on heating. Four temperature values are in the biphasic region: two on one side of the N_{tb}–N_u phase transition and two on the other (see text for details).

5 Conclusions

EPR spectra of the CSL spin probe dissolved in the nematic phases exhibited by the CB11CB liquid crystal confirmed the presence of an higher temperature uniaxial nematic phase and of a lower temperature nematic phase in which the director distribution is not uniform. This lower temperature nematic phase has been recently described as a twist-bend phase[6,8,10,12,27,39] where the local nematic domain director precesses uniformly about an axis, making a fixed angle, θ_0, with it. The EPR spin probe technique is particularly suitable to examine the differences between the orientational order $\langle P_2 \rangle$ with respect to a local director as well as the distribution of local domains, characterized by a director order parameter $\langle P_2 \rangle_d$. This could be particularly important when $\langle P_2 \rangle_d$ is very different from one, i.e. the sample is not a monodomain. The limiting case is that of an isotropic distributions of domains, like in a spherical membrane vesicle[52] or in a macroscopically isotropic LC elastomer[53], where the local domains are ordered, but the overall macroscopic order in the laboratory frame is vanishing. Thus the EPR spin probe method has some advantages on techniques like birefringence that measure the overall order of the sample in the laboratory frame. Moreover, the magnetic field employed in EPR is much lower than that used in NMR, so that a sample aligned beforehand in a strong field can actually be rotated during the experiment and spectra at various angles (here parallel and perpendicular to the field) recorded. To analyse the EPR spectra, a fixed-tilt (FT) model and a distributed-tilt (DT) model have been developed here to calculate the spectra expected in the twist-bend phase. Experimental spectra of samples in which the twist-bend axis should be parallel to the magnetic field showed marked differences from the spectra calculated according to the FT model but were, instead, well reproduced by the DT model.

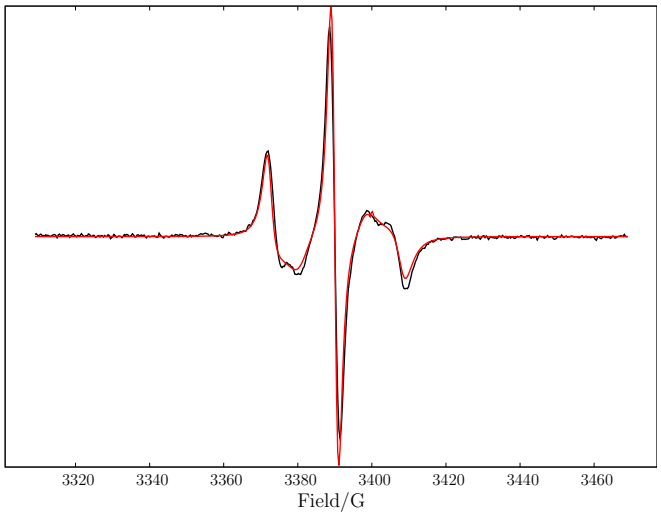

Fig. 11 EPR spectrum (black line) at 371.7 K in the supercooled N_{tb} phase, and fit (red line) in the assumption that the local $\langle P_2 \rangle$ is described by the Haller function shown as a dashed line in Figure 9 (see text for details).

This distribution, reported by the spin probe, is expected to be a relatively accurate description of the actual local director distribution in the twist-bend phase. The macroscopic monodomain observed in the N_u phase and the fact that the values of $\langle P_2 \rangle$ recovered from the analyses are in good agreement with those observed in a recent study of CB11CB[48] indicate that the spin probe is able to report quite accurately the overall orientation of the LC molecules, as in previous studies of uniaxial nematics[33,45,54].

On the other hand, the EPR spin probe technique can only provide insights about the actual geometry of the twist-bend nematic phase. Our present results suggest that the tilt angle of the local director in the N_{tb} phase is not fixed but that a relatively narrow distribution of tilt angles with $\langle P_2 \rangle_d$ around 0.5–0.6 is present. This observation would not be compatible with a model of the phase in which the helical axis is macroscopically straight and the tilt angle fixed. However, our results do not exclude other similar organizations. In particular the possibility of the conic angle not being unique, but rather of varying with the molecular segments of the dimers has been recently put forward by Vanakaras and Photinos[22] and could provide a possible molecular origin of the tilt distribution as reported by the CSL spin probe. A discussion about a possible more complex structure of the twist-bend phase of CB11CB has also been recently provided by Mandle et al.[9], while yet another possibility, recently put forward, is that the axis of the helix is not fixed but undulates[42]. Our data cannot positively distinguish between these different models at this stage, but we hope that this work will stimulate further analysis of these very interesting phases.

6 Acknowledgements

We thank MIUR, EU-BIND (FP7-216025), the University of Bologna and the CINFO Computer Centre, University of Camerino for support.

References

1 V. P. Panov, M. Nagaraj, J. K. Vij, Y. P. Panarin, A. Kohlmeier, M. G. Tamba, R. A. Lewis and G. H. Mehl, *Phys. Rev. Lett.*, 2010, **105**, 167801 1–4.

2 M. Cestari, S. Diez-Berart, D. A. Dunmur, A. Ferrarini, M. R. de la Fuente, D. J. B. Jackson, D. O. Lopez, G. R. Luckhurst, M. A. Perez-Jubindo, R. M. Richardson, J. Salud, B. A. Timimi and H. Zimmermann, *Phys. Rev. E*, 2011, **84**, 031704 1–20.

3 R. B. Meyer, in *Molecular Fluids*, ed. R. Balian and G. Weil, Gordon and Breach, New York, 1976, vol. XXV of Les Houches Summer School in Theoretical Physics, pp. 272–373.

4 I. Dozov, *Europhys. Lett.*, 2001, **56**, 247–253.

5 L. Beguin, J. W. Emsley, M. Lelli, A. Lesage, G. R. Luckhurst, B. A. Timimi and H. Zimmermann, *J. Phys. Chem. B*, 2012, **116**, 7940–7951.

6 C. Greco, G. R. Luckhurst and A. Ferrarini, *Phys. Chem. Chem. Phys.*, 2013, **15**, 14961–14965.

7 C. Meyer, G. R. Luckhurst and I. Dozov, *Phys. Rev. Lett.*, 2013, **111**, 067801 1–5.

8 V. Borshch, Y. K. Kim, J. Xiang, M. Gao, A. Jakli, V. P. Panov, J. K. Vij, C. T. Imrie, M. G. Tamba, G. H. Mehl and O. D. Lavrentovich, *Nat. Commun.*, 2013, **4**, 2635 1–8.

9 R. J. Mandle, E. J. Davis, C. T. Archbold, S. J. Cowling and J. W. Goodby, *J. Mater. Chem. C*, 2014, **2**, 556–566.

10 D. Chen, J. H. Porada, J. B. Hooper, A. Klittnick, Y. Shen, M. R. Tuchband, E. Korblova, D. Bedrov, D. M. Walba, M. A. Glaser, J. E. Maclennan and N. A. Clark, *Proc. Natl. Acad. Sci. U. S. A.*, 2013, **110**, 15931–15936.

11 M. Gao, Y.-K. Kim, C. Zhang, V. Borshch, S. Zhou, H.-S. Park, A. Jakli, O. D. Lavrentovich, M.-G. Tamba, A. Kohlmeier, G. H. Mehl, W. Weissflog, D. Studer, B. Zuber, H. Gnaegi and F. Lin, *Microsc. Res. Tech.*, 2014, **77**, 754–772.

12 C. Meyer, G. R. Luckhurst and I. Dozov, *J. Mater. Chem. C*, 2015, **3**, 318–328.

13 M. Tamba, S. Salili, C. Zhang, A. Jakli, G. Mehl, R. Stannarius and A. Eremin, *RSC Advances*, 2015, **5**, 11207–11211.

14 R. J. Mandle, E. J. Davis, C.-C. A. Voll, C. T. Archbold, J. W. Goodby and S. J. Cowling, *Liq. Cryst.*, 2015, **42**, 688–703.

15 R. J. Mandle, E. J. Davis, C. T. Archbold, C. C. A. Voll, J. L. Andrews, S. J. Cowling and J. W. Goodby, *Chem.-Eur. J.*, 2015, **21**, 8158–8167.

16 C. Greco, G. R. Luckhurst and A. Ferrarini, *Soft Matter*, 2014, **10**, 9318–9323.

17 Z. Lu, P. A. Henderson, B. J. A. Paterson and C. T. Imrie, *Liq. Cryst.*, 2014, **41**, 471–483.

18 R. J. Mandle, E. J. Davis, S. A. Lobato, C. C. A. Vol, S. J. Cowling and J. W. Goodby, *Phys. Chem. Chem. Phys.*, 2014, **16**, 6907–6915.

19 D. Chen, M. Nakata, R. Shao, M. R. Tuchband, M. Shuai, U. Baumeister, W. Weissflog, D. M. Walba, M. A. Glaser, J. E. Maclennan and N. A. Clark, *Phys. Rev. E*, 2014, **89**, 022506 1–5.

20 A. Hoffmann, A. G. Vanakaras, A. Kohlmeier, G. H. Mehl and D. J. Photinos, *Soft Matter*, 2015, **11**, 850–855.

21 E. Gorecka, M. Salamonczyk, A. Zep, D. Pociecha, C. Welch, Z. Ahmed and G. Mehl, *Liq. Cryst.*, 2015, **42**, 1–7.

22 A. Vanakaras and D. Photinos, *Soft Matter*, 2016, **12**, 2208–2220.

23 G. Barbero, L. Evangelista, M. Rosseto, R. Zola and I. Lelidis, *Phys. Rev. E*, 2015, **92**, 030501 1–5.

24 J. H. Freed, in *Spin Labeling. Theory and Applications*, ed. L. J. Berliner, Academic Press, New York, 1976, ch. 3, pp. 53–132.

25 C. Bacchiocchi, I. Miglioli, A. Arcioni, I. Vecchi, K. Rai, A. Fontecchio and C. Zannoni, *J. Phys. Chem. B*, 2009, **113**, 5391–5402.

26 H. Gopee, A. Cammidge and V. Oganesyan, *Angew. Chem. Int. Ed.*, 2013, **52**, 8917–8920.

27 J. P. Jokisaari, G. R. Luckhurst, B. A. Timimi, J. Zhu and H. Zimmermann, *Liq. Cryst.*, 2015, **42**, 708–721.

28 R. Balachandran, V. P. Panov, J. K. Vij, A. Kocot, M. G. Tamba, A. Kohlmeier and G. H. Mehl, *Liq. Cryst.*, 2013, **40**, 681–688.

29 R. Balachandran, V. P. Panov, Y. P. Panarin, J. K. Vij, M. G. Tamba, G. H. Mehl and J. K. Song, *J. Mater. Chem. C*, 2014, **2**, 8179–8184.

30 R. Balachandran, V. P. Panov, Y. P. Panarin, M. G. Tamba, G. H. Mehl, J. K. Song and J. K. Vij, *Mol. Cryst. Liquid Cryst.*, 2015, **611**, 65–70.

31 E. Meirovitch and J. H. Freed, *J. Phys. Chem.*, 1984, **88**, 4995–5004.

32 A. Arcioni, C. Bacchiocchi, I. Vecchi, G. Venditti and C. Zannoni, *Chem. Phys. Lett.*, 2004, **396**, 433–441.

33 I. Vecchi, A. Arcioni, C. Bacchiocchi, G. Tiberio, P. Zanirato and C. Zannoni, *J. Phys. Chem. B*, 2007, **111**, 3355–3362.

34 S. G. Carr, S. K. Khoo, G. R. Luckhurst and C. Zannoni, *Molec. Cryst. Liq. Cryst.*, 1976, **35**, 7–13.

35 J. H. Freed, in *Electron Spin Relaxation in Liquids*, ed. L. T. Muus and P. W. Atkins, Plenum Press, New York, 1972, ch. 14, pp. 387–409.

36 D. J. Schneider and J. H. Freed, in *Spin Labeling. Theory and Applications*, ed. L. J. Berliner and J. Reuben, Plenum Press, New York, 1989, vol. 8 of Biological Magnetic Resonance, ch. 1, pp. 1–76.

37 A. Arcioni, R. Tarroni and C. Zannoni, *J. Chem. Soc.-Faraday Trans.*, 1993, **89**, 2815–2822.

38 P. R. Bevington, *Data Reduction and Error Analysis for the Physical Sciences*, McGraw-Hill, New York, 1969.

39 E. G. Virga, *Phys. Rev. E*, 2014, **89**, 052502 1–10.

40 D. Budil, S. Lee, S. Saxena and J. Freed, *J. Magn. Reson. Ser. A*, 1996, **120**, 155–189.

41 J. Berntsen, T. O. Espelid and A. Genz, *ACM Trans. Math. Softw.*, 1991, **17**, 452–456.

42 P. K. Challa, V. Borshch, O. Parri, C. T. Imrie, S. N. Sprunt, J. T. Gleeson, O. D. Lavrentovich and A. Jakli, *Phys. Rev. E*, 2014, **89**, 060501 1–5.

43 C. Bacchiocchi, I. Miglioli, A. Arcioni, K. Rai, A. Fontecchio and C. Zannoni, *Mol. Cryst. Liquid Cryst.*, 2012, **558**, 127–139.

44 C. Bacchiocchi, G. Foschi, I. Miglioli, S. Shoarinejad, A. Arcioni and C. Zannoni, *Mol. Cryst. Liquid Cryst.*, 2015, **614**, 2–10.

45 V. Oganesyan, E. Kuprusevicius, H. Gopee, A. Cammidge and M. Wilson, *Phys. Rev. Lett.*, 2009, **102**, 013005 1–4.

46 J. W. Emsley, P. Lesot, G. R. Luckhurst, A. Meddour and D. Merlet, *Phys. Rev. E*, 2013, **87**, 040501 1–4.

47 C. S. P. Tripathi, P. Losada-Pérez, C. Glorieux, A. Kohlmeier, M.-G. Tamba, G. H. Mehl and J. Leys, *Phys. Rev. E*, 2011, **84**, 041707 1–7.

48 Z. Zhang, V. P. Panov, M. Nagaraj, R. J. Mandle, J. W. Goodby, G. R. Luckhurst, J. C. Jones and H. F. Gleeson, *J. Mater. Chem. C*, 2015, **3**, 10007–10016.

49 J. W. Emsley, M. Lelli, H. Joy, M. G. Tamba and G. H. Mehl, *Phys. Chem. Chem. Phys.*, 2016, **18**, 9419–9430.

50 I. Haller, *Prog. Solid State Ch.*, 1975, **10**, 103–118.

51 C. Meyer, G. Luckhurst and I. Dozov, *J. Mat. Chem.*, 2015, **3**, 318–328.

52 C. Zannoni, G. F. Pedulli, L. Masotti and A. Spisni, *J. Mag. Res.*, 1981, **43**, 141–153.

53 G. Skacej and C. Zannoni, *Macromolecules*, 2014, **47**, 8824–8832.

54 A. Arcioni, C. Bacchiocchi, L. Grossi, A. Nicolini and C. Zannoni, *J. Phys. Chem. B*, 2002, **106**, 9245–9251.

Detailed EPR spectral analyses suggest a distributed rather than a fixed tilt angle in the twist-bend nematic phase.